Highly anisotropic crystal growth and thermoelectric properties of $K_2Bi_{8-x}Sb_xSe_{13}$ solid solutions: Band gap anomaly at low x

Theodora Kyratsi[a)]
Department of Chemistry, Michigan State University, East Lansing, Michigan 48824

Jeffrey S. Dyck and Wei Chen
Department of Physics, University of Michigan, Ann Arbor, Michigan 48109

Duck-Young Chung
Department of Chemistry, Michigan State University, East Lansing, Michigan 48824

Ctirad Uher
Department of Physics, University of Michigan, Ann Arbor, Michigan 48109

Konstantinos M. Paraskevopoulos
Department of Physics, Aristotle University of Thessaloniki, 54006 Thessaloniki, Greece

Mercouri G. Kanatzidis[b)]
Department of Chemistry, Michigan State University, East Lansing, Michigan 48824

(Received 4 February 2002; accepted for publication 8 April 2002)

The thermoelectric properties of solid solutions of the type β-$K_2Bi_{8-x}Sb_xSe_{13}$ ($0<x<8$) were studied with respect to thermal behavior, band gap variation, and charge transport properties as a function of x. At x values between 0 and 1.5, the energy band gap is observed to decrease (anomalous) before it widens with increasing x values as would be expected. For selected members of the solid solutions, the Bridgman technique was applied to obtain well-grown oriented ingots that were used to measure the thermal conductivity and charge transport properties in different growth directions. The measurements showed a strong anisotropy in thermoelectric properties with the largest anisotropy observed in the electrical conductivity. Lattice thermal conductivities of the selected solid solutions were observed to decrease when the x value increases. Preliminary doping studies on the $x=1.6$ member were carried out and it was shown that it is possible to significantly increase the power factor. [DOI: 10.1063/1.1481967]

I. INTRODUCTION

Candidate materials for thermoelectric applications should possess high electrical conductivity, high Seebeck coefficient, and low thermal conductivity, so that the thermoelectric figure of merit ZT can be maximized.[1] To increase ZT, it is necessary either to increase the power factor ($\sigma \cdot S^2$), or decrease the thermal conductivity or both. As suggested by the Mott formula,[2] materials with electronic complexities near the Fermi level have a good chance to possess high Seebeck coefficient. On the other hand, decrease of the lattice thermal conductivity can be accomplished with materials that fit the concept of ''phonon glass electron crystal'' [3] through ''rattling'' atoms in cages or tunnels of the structure, or by materials with complex compositions, large unit cells, low crystal symmetry, and site occupancy disorder provided. The latter can be provided through the mixed occupation of different atoms in a series of solid solutions (e.g., $Bi_{2-x}Sb_xTe_3$).

Our investigations of ternary and quaternary compounds of bismuth chalcogenides[4] have shown that several multinary compounds containing alkali metals present promising thermoelectric properties. Alkali metals tend to create structural complexity in the crystal that can lead to complex electronic structure. Additionally, they reside between layers or in tunnels created by covalent frameworks and because they are ionically interacting with the framework they tend to rattle as revealed by their high thermal displacement parameters.[5] The structure of β-$K_2Bi_8Se_{13}$ (Ref. 6) presents several key characteristics that include two different interconnected types of Bi/Se blocks, K ions positionally and compositionally disordered with Bi or other K atoms, over the same crystallographic sites, and loosely bound K atoms in tunnels. These features seem to be responsible for the low thermal conductivity of this compound ($\sim$1.3 W/m K).[6] Doping studies on β-$K_2Bi_8Se_{13}$ have shown that its ZT can be substantially improved, mainly by raising the power factor.[7]

In this work, β-$K_2Bi_8Se_{13}$ was alloyed with its isostructural $K_2Sb_8Se_{13}$ analog[6] to produce a series of compounds with the formula $K_2Bi_{8-x}Sb_xSe_{13}$. The Sb/Bi substitution was performed in order to generate extensive mass fluctuations in the lattice of β-$K_2Bi_8Se_{13}$ and to study the effect of these fluctuations on the thermal and charge transport properties of these materials. We find that the band gaps and the melting points vary systematically as a function of x. Various $K_2Bi_{8-x}Sb_xSe_{13}$ solid solutions were prepared with the Bridgman technique[8] in order to grow large highly oriented

[a)]Also at: Department of Physics, Aristotle University of Thessaloniki, 54006 Thessaloniki, Greece.
[b)]Electronic mail: kanatzid@cem.msu.edu

ingot samples so we could study the effects of the crystal orientation and composition (i.e., value of x) on the lattice thermal conductivity and the power factor. Indeed, these materials showed strong anisotropy in their thermoelectric performance. Doping studies using excess of Se were performed on selected solid solution members in order to study the variation of the thermoelectric properties. Preliminary doping studies using varying amounts of excess Se, Pb, and Sn were also performed on one solid solution member.

II. EXPERIMENTAL SECTION

A. Reagents

Chemicals used in this work were generously provided by Tellurex Inc. as obtained: bismuth chunks (99.999%), antimony chunks (99.999%), selenium shots (99.999%), and potassium chunks (98% Aldrich Chemical Co., Inc., Milwaukee, WI).

B. Synthesis and crystal growth

All manipulations were carried out under a dry nitrogen atmosphere in a Vacuum Atmospheres Dri-Lab glovebox.

(1) β-$K_2Bi_8Se_{13}$: A mixture of potassium metal (0.282 g. 7.2 mmol), bismuth (6.021 g, 28.8 mmol), and selenium (3.697 g, 46.8 mmol) was loaded into a silica tube and subsequently flame sealed at a residual pressure of $<10^{-4}$ Torr. The mixture was heated to 850 °C over 12 h and kept there for 1 h, followed by cooling to 450 °C and kept there for 48 h and cooling at 50 °C at a rate of ~15 °C/h. The mixture was annealed at 450 °C for 48 h in order to have pure β-$K_2Bi_8Se_{13}$ phase products.

(2) $K_2Sb_8Se_{13}$: A mixture of potassium metal (0.376 g, 9.6 mmol), antimony (4.686 g, 38.5 mmol), and selenium (4.938 g, 62.5 mmol) was loaded into a silica tube and subsequently flame sealed at a residual pressure of $<10^{-4}$ Torr. The mixture was heated to 850 °C over 12 h and kept there for 1 h, followed by cooling to 50 °C at a rate of ~15 °C/h. The desired phase was obtained with >95% purity.

(3) $K_2Bi_{8-x}Sb_xSe_{13}$: Mixtures of β-$K_2Bi_8Se_{13}$ and $K_2Sb_8Se_{13}$ in various proportions were loaded into a silica tube and subsequently flame sealed at a residual pressure of $<10^{-4}$ Torr. The mixtures were heated to 850 °C over 12 h and kept there for 1 h, followed by cooling to 50 °C at a rate of ~15 °C/h. For example, $K_2Bi_{8-x}Sb_xSe_{13}$ ($x=1.6$) was prepared by mixing 7 g $K_2Bi_8Se_{13}$ (2.52 mmol) and 1.310 g $K_2Sb_8Se_{13}$ (0.63 mmol). Some of the samples were prepared by mixing potassium metal, bismuth, antimony, and selenium. For example $K_2Bi_{8-x}Sb_xSe_{13}$ ($x=1.6$) with 0.2% Se excess was prepared by mixing 0.271 g K (6.9 mmol), 5.086 g Bi (24.3 mmol), 0.741 g Sb (6.1 mmol), and 3.911 g Se (49.5 mmol).

Highly oriented crystal ingots of selected composition of $K_2Bi_{8-x}Sb_xSe_{13}$ were grown with modified Bridgman technique. They were obtained by recrystallizing $K_2Bi_{8-x}Sb_xSe_{13}$ in a vertical single-zone furnace, with a temperature gradient of ~15 °C/cm. The material was placed in a rounded bottom silica tube and 9 mm outer diameter, and flame sealed under vacuum ($<10^{-4}$ Torr). The tube was lowered through the temperature gradient profile with a dropping rate of ~0.3 cm/h.

Scanning electron microscopy/energy dispersive spectroscopy (SEM/EDS) analysis on different spots along the ingots showed that products were pure with no variation of x. For example, analysis at different spots along the oriented ingot for member $x=4$ showed 8.5 ± 1.5 wt % K, 17.9 ± 2 wt % Bi, 17.5 ± 1.5 wt % Sb, and 56 ± 2 wt % Se.

C. Electron microscopy

Quantitative microprobe analyses and crystal imaging of the compounds were performed with a JEOL JSM-35C scanning electron microscope equipped with a Tracor Northern EDS detector. Data were acquired using an accelerating voltage of 20 kV and a 1 min accumulation time. The compositions reported here are the result of averaging a large number of independent measurements from a given sample.

D. Differential thermal analysis

Differential Thermal Analysis (DTA) was performed with a computer-controlled Shimadzu DTA-50 thermal analyzer. The ground single crystals (~30 mg total mass) were sealed in silica ampoules under a vacuum. A silica ampoule containing alumina of equal mass was sealed and placed on the reference side of the detector. The samples were heated to 850 °C at 10 °C/min where isothermed for 5 min followed by cooling at 10 °C/min to room temperature and finally this cycle was repeated. The DTA sample was examined with powder x-ray diffraction after the experiment.

E. Infrared and ultraviolet/visible spectroscopy

Optical diffuse reflectance measurements were carried out on finely ground samples at room temperature. The spectra were recorded, in the infrared region (6000–400 cm^{-1}), with the use of a Nicolet MAGNA-IR 750 Spectrometer equipped with a diffuse reflectance attachment from Spectra-Tech. Inc. In the 200–2500 nm region, optical diffuse reflectance measurements were also performed at room temperature in a Shimadzu UV-3101 PC double-beam, double-monochromator spectrophotometer, equipped with an integrating sphere. The measurement of diffuse reflectivity can be used to obtain values for the band gap that agree rather well with the values obtained by transmission measurements from single crystals of the same material. Absorption (α/S) data were calculated from the reflectance data using Kubelka–Munk[9] function: $\alpha/S=(1-R)^2/2R$, where R is the reflectance at a given wavenumber, α is the absorption coefficient, and S is the scattering coefficient. The scattering coefficient has been shown[9] to be practically wave number independent for particles larger than 5 μm, which is smaller than the particles size of the samples used in this work. The band gap was determined as the intersection point between energy axis at the absorption offset and the line extrapolated from the linear absorption edge in a α/S versus E (eV) plot.

F. Charge-transport and thermal conductivity measurements

Electrical resistivity was measured using a Linear Research ac bridge with 16 Hz excitation in a cryostat equipped with a magnet capable of fields up to 5.5 T. Thermal conductivity and Seebeck coefficient were determined using a longitudinal steady-state method over the temperature range 4–300 K. In this case, samples were attached (using either a low melting point solder or silver-loaded epoxy) to the cold tip of the cryostat, while the other end of the sample was provided with a small strain gauge resistor (thin film), which serves as a heater. The temperature difference across the sample was measured using differential chromel-constantan thermocouple. The Seebeck voltage was measured with thin copper wire the thermopower of which was calibrated against a high-T_C superconductor up to 134 K.

The samples for the charge-transport, thermal conductivity, and Hall effect measurements were cut in about $3\times3\times5\ \mathrm{mm}^3$ dimensions with the 5 mm length along the needle direction, using precision saw ISOMET low speed saw, attached with diamond blade of 10.2 cm diameter and 0.3 mm thickness.

G. Powder x-ray diffraction

The solid solutions were examined by x-ray powder diffraction to assess phase purity, for identification and determination of the lattice parameters. Powder patterns were obtained using a Rigaku Rotaflex powder x-ray diffractometer with Ni-filtered Cu Kα radiation operating at 45 kV and 100 mA. The data were collected at a rate of 2 °/min. The purity of phases for the solid solutions was confirmed by comparison of x-ray powder diffraction pattern to the calculated one from single-crystal data for β-$K_2Bi_8Se_{13}$ using Cerius[2] software.[10]

III. RESULTS AND DISCUSSION

A. Sample preparation and thermal analysis

β-$K_2Bi_8Se_{13}$ is formed as an ingot by reacting a stoichiometric combination of potassium metal, bismuth, and selenium at 850 °C. The products, however, tend to have $K_{2.5}Bi_{8.5}Se_{14}$ phase[6] as an impurity (~20%) because these two phases are closely related in composition and structure and are both formed under similar conditions. A pure phase of β-$K_2Bi_8Se_{13}$ can be produced by annealing treatment of the mixed-phase product at 450 °C for more than 48 h. $K_2Sb_8Se_{13}$ was easily formed as a single-phase product by a stoichiometric reaction at 850 °C.

To prepare the $K_2Bi_{8-x}Sb_xSe_{13}$ ($0<x<8$) solid solutions β-$K_2Bi_8Se_{13}$ and $K_2Sb_8Se_{13}$ were mixed in various proportions at 850 °C. Some of the samples were prepared by reacting a stoichiometric combination of potassium metal, bismuth, antimony, and selenium at 850 °C. The solid solutions were obtained as a pure phase, which was confirmed by powder x-ray diffraction, making additional thermal treatments unnecessary. From these reactions, it appears that the introduction of Sb metal favors the formation of the β-$K_2Bi_8Se_{13}$ structure type and avoids the $K_{2.5}Bi_{8.5}Se_{14}$ phase.

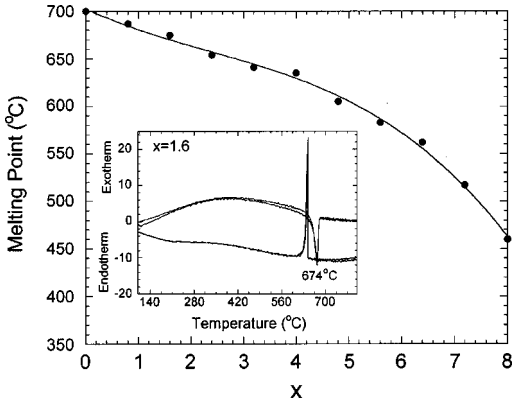

FIG. 1. Melting points of the $K_2Bi_{8-x}Sb_xSe_{13}$ solid solutions vs x and differential thermal analysis (inset) for member $x=1.6$ showing the melting and crystallization events.

The melting points of the end members β-$K_2Bi_8Se_{13}$ and $K_2Sb_8Se_{13}$ were found to be 700 °C and 460 °C, respectively. The solid solutions have melting points in between with no eutectic composition present, see Fig. 1. The monotonic decrease of melting points indicates the incorporation of Sb in the β-$K_2Bi_8Se_{13}$ phase.

B. Energy gap dependence on concentration—Anomalous behavior at low *x*

The semiconducting energy gaps, E_g, of the end members and solid solutions were determined optically at room temperature using mid and near-infrared spectroscopy. The energy gaps were manifest themselves as well defined and abrupt changes in the absorption coefficient [Fig. 2(a) for $x=1.6$]. Given that energy gaps of the end members $K_2Bi_8Se_{13}$ and $K_2Sb_8Se_{13}$ are 0.59 eV and 0.78 eV respectively,[6] a gradual increase of the band gap of the $K_2Bi_{8-x}Sb_xSe_{13}$ solid solutions with increasing Sb participation would be expected. However, it is surprising to observe that small amounts of Sb incorporation into the $K_2Bi_8Se_{13}$ structure actually cause the E_g to decrease, slightly but discernibly, achieving a minimum of 0.57 eV at $x\sim1.5$, see Fig. 2(b). The significant increase in E_g actually starts when Sb atoms replace >30% of Bi atoms. This implies that up to 30% Sb incorporation ($x\approx2.5$) does not disturb significantly the energy bands close to Fermi level.

In order to understand the anomaly in E_g variation with x, it is essential to consider the crystal structure of β-$K_2Bi_8Se_{13}$, which is made of infinite $NaCl^{111}$-type rods arranged side by side to form layers perpendicular to the c axis, Fig. 3. Then infinite rods of NaCl-type connect the layers to build a three-dimensional (3D) framework, which creates the needlelike crystal morphology, with tunnels filled with K^+ cations. In a previous single-crystal analysis study of solid solution members with $x=4.0$ and 2.4, we learned that the Sb incorporation into this lattice is in fact nonuniform.[11] The most susceptible sites in the structure to accept Sb atoms are the potassium $K1$ and $M8$ sites [here

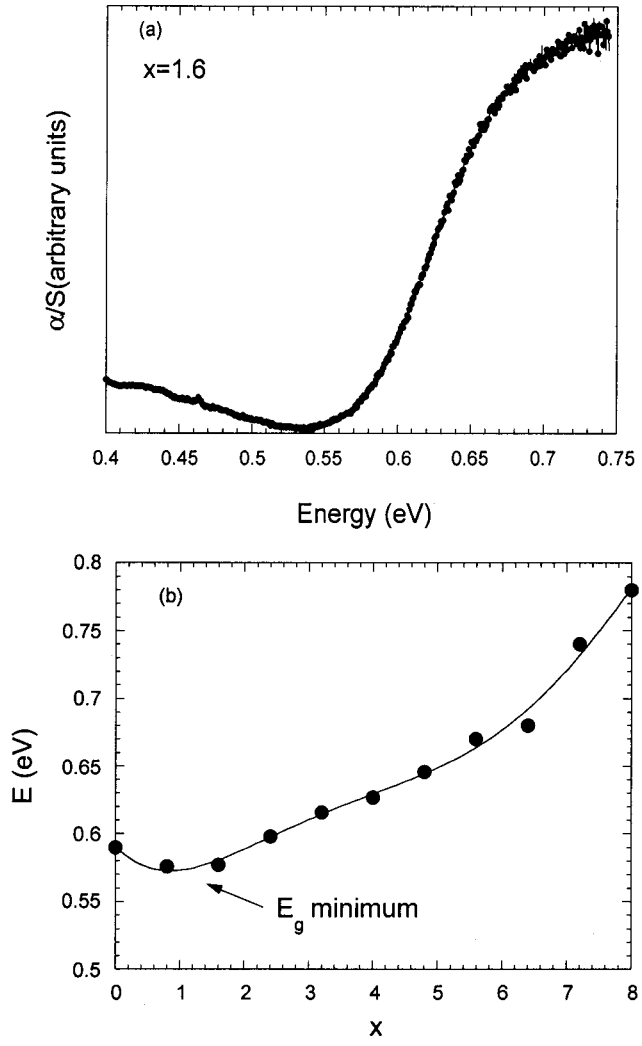

FIG. 2. (a) Representative infrared absorption spectrum of $K_2Bi_{8-x}Sb_xSe_{13}$ ($x=1.6$) showing band gap of 0.58 eV. (b) Variation of the energy gap with x in the $K_2Bi_{8-x}Sb_xSe_{13}$ solid solutions.

fully occupied by Sb, Sb(8)] which appear to be the first to fill with Sb, see Fig. 3. Therefore, the slight narrowing of the energy gap may be due to the fact that Sb initially affects sites occupied by K (i.e., $K1$ sites). The K^+ ions are simply spectator ions not contributing significantly to the electronic structure at the Fermi level because they are only ionically interacting with the $[Bi_8Se_{13}]^{2-}$ framework. Their valence s and p orbital energies lie very high and away from those of Bi and Se atoms. This is not the case with Sb^{3+} ions however, and any substitution on a K site will generate substantial covalent interactions with the $[Bi_8Se_{13}]^{2-}$ framework thus altering the electronic structure at the Fermi level through band broadening consequently reducing the energy gap. On the other hand, substitution of Sb on a Bi site of β-$K_2Bi_8Se_{13}$, which happens as x increases, has a completely different effect. Antimony atoms are smaller than Bi atoms and possess lower-energy atomic orbitals, which can lead to wider energy gap by lowering the top of the valence band and more importantly raising the bottom of the conduction band. In this case, the factors operating are the same as those responsible for increasing the E_g in going from Bi_2Se_3

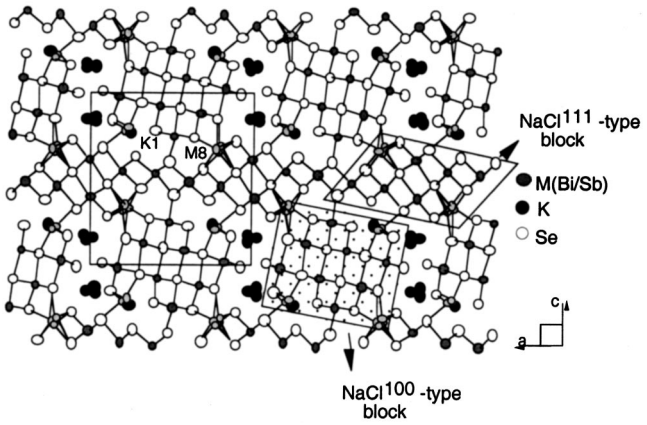

FIG. 3. The crystal structure of $K_2Bi_{8-x}Sb_xSe_{13}$ ($x=4.0$ and 2.4) with atom labeling showing the $K1$ and $M8$ sites. These sites are the first to be substituted with Sb.

($E_g\sim0.3$ eV)[12] to Sb_2Se_3 ($E_g\sim1.1$ eV),[13] from Bi_2Te_3 ($E_g\sim0.13$ eV) to Sb_2Te_3 ($E_g\sim0.28$ eV),[13] or β-$K_2Bi_8Se_{13}$ ($E_g\sim0.59$ eV) to $K_2Sb_8Se_{13}$ ($E_g\sim0.78$ eV).

C. Lattice parameters

The lattice parameters of various members of $K_2Bi_{8-x}Sb_xSe_{13}$ solid solutions series were determined using the experimental powder diffraction patterns and were refined with the program U-FIT.[14] The composition dependence of the unit cell volume is shown in Fig. 4. The volume decreases as Sb participation increases as expected due to its smaller size. The slope of the variation seems greater for low Sb concentration ($x<2$) than for high Sb concentration i.e., $x>2$. Again, this change in slope is due to the preference of Sb atoms to occupy the high coordinated sites [$M(8)$ and $K(1)$] of the structure[11] first. Thus, the concentration of the unit cell is faster at the early stages of Sb substitution ($x<2$). For $x>2$, Bi/Sb distribution is random on the other heavy metal octahedral sites. In this range the unit cell volume variation follows Vegard's law, which is the typical behavior for solid solutions.

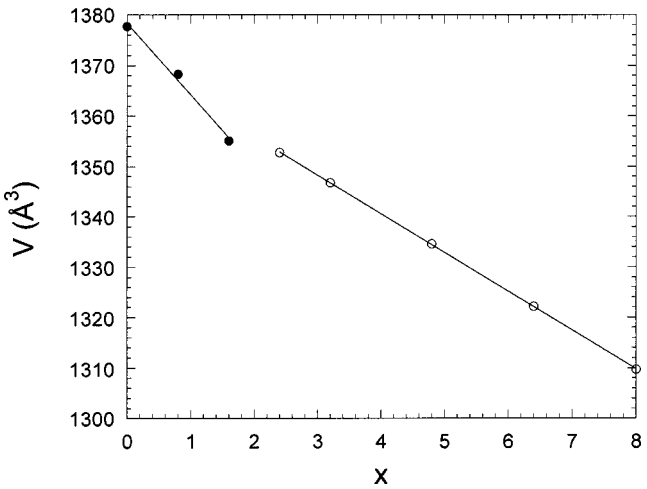

FIG. 4. Variation of the volume of the unit cell with x in the $K_2Bi_{8-x}Sb_xSe_{13}$ solid solutions.

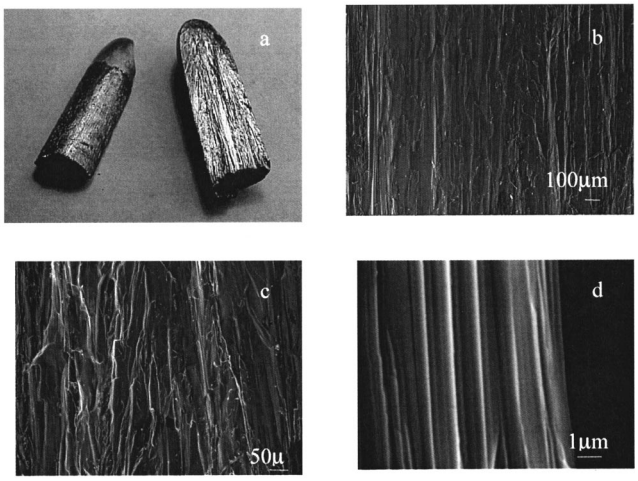

FIG. 5. (a) Photo of the broken ingot of $K_2Bi_{8-x}Sb_xSe_{13}$ ($x=1.6$) and (b) SEM photo for its inside surface. (c) SEM photo of the inside surface of a broken ingot of $K_2Bi_{8-x}Sb_xSe_{13}$ ($x=2.4$) and (d) its high magnification SEM photo showing long smooth fiberlike morphology typical of the entire bodies of the ingots. The presence of many needle boundaries perpendicular to the growth direction is evident.

D. Crystal growth

Because the $K_2Bi_{8-x}Sb_xSe_{13}$ solid solutions grew well as highly oriented dense polycrystalline ingots, using a modified vertical drop Bridgman technique, they presented an excellent opportunity to study not only the electrical and thermal transport properties as a function of x, but also the directional anisotropy in these properties. Selected compositions of $K_2Bi_{8-x}Sb_xSe_{13}$ ($0<x<4$) solid solutions were prepared and grown[15] as large ingots (~3 cm). The ingots consisted of well-oriented needlelike crystals parallel to the sample translation axis. The samples show excellent directionally solidifying properties with the crystal needles often spanning the length of the grown ingot, Fig. 5(a) (for $x=1.6$). The SEM photo in Fig. 5(b) shows the inside surface of a broken ingot; Fig. 5(c) shows the needles of a highly oriented part of the ingot (for $x=2.4$) and its high magnification SEM photo showing long smooth fiber like morphology is shown in Fig. 5(d). The ingots were cut with a diamond blade saw to obtain specimens parallel and perpendicular to the growth axis exposure. Peak indexed x-ray diffraction profiles associated with the two different ingot orientations of the $K_2Bi_{8-x}Sb_xSe_{13}$ ($x=1.6$) sample are shown in Fig. 6. The lack of simultaneous occurrence of peaks in the two diffraction patterns indicates an extremely high degree of orientation (>95%). Diffraction profiles from specimens, with exposed surface parallel to growth axis, consist of ($h0l$) reflections [Fig. 6(a)] while (020) reflection becomes the strongest on the other direction [exposed surface perpendicular to growth axis, Fig. 6(b)].

E. Charge transport properties

Electrical conductivity measurements on $K_2Bi_{8-x}Sb_xSe_{13}$ solid solutions were carried out along the needle direction (i.e., crystallographic b axis) for the members of $x=0.8$ and $x=1.6$. The electrical conductivity has a

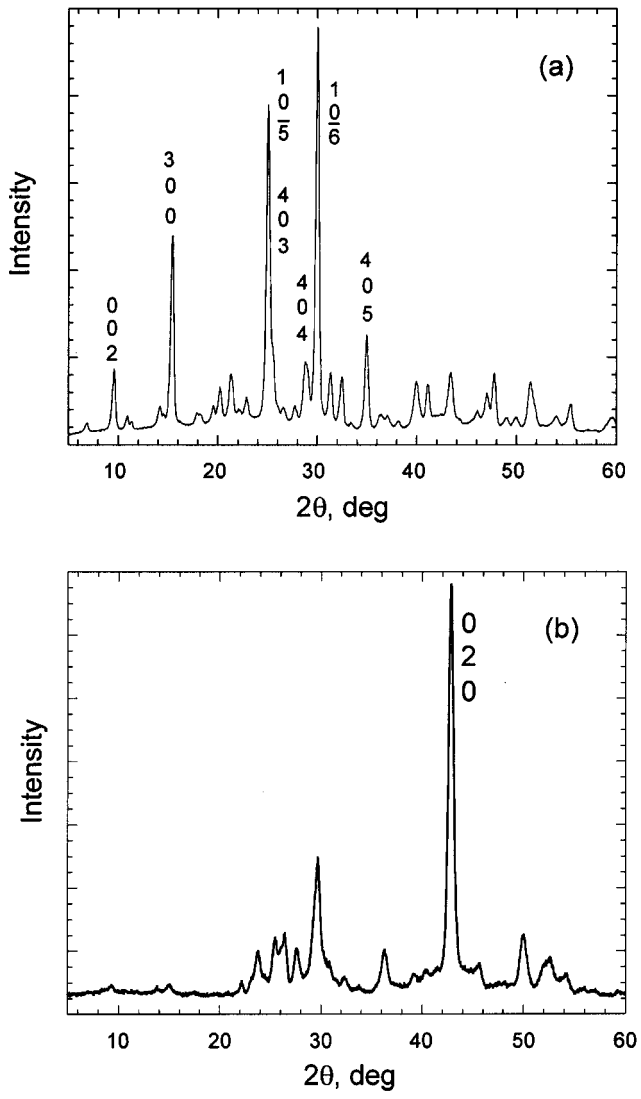

FIG. 6. X-ray diffraction pattern of $K_2Bi_{8-x}Sb_xSe_{13}$ ($x=1.6$) sample exposed parallel (a) and perpendicular (b) to growth direction (Cu $K\alpha$ radiation).

weak negative temperature dependence, consistent with a semimetal or a narrow-gap semiconductor behavior, see Fig. 7. In going from $x=0.8$ to $x=1.6$, the room-temperature values increase from 55 to 292 S/cm. The observed differences in these two samples can be understood from the Hall effect measurements.

The Hall coefficient values (R_H) for both members were negative in sign, indicating electrons as the major charge carrier (n type) in agreement with the observed negative Seebeck coefficients (see next). Interestingly, all bismuth selenide based materials that we are aware of possess electrons as the major charge-transport carrier (n type) whereas p-type materials are virtually unknown. The carrier concentration was calculated [$R_H=1/(n\cdot e)$] to be $\sim 1.6\times 10^{20}$ cm^{-3} for $x=0.8$ and $\sim 1.1\times 10^{20}$ cm^{-3} for $x=1.6$, Fig. 8. These values indicate that the ''as-prepared'' samples were in a relatively highly doped state. This is supported by the fact that the carrier concentration shows very little dependence with the temperature, which indicates the absence of band to band

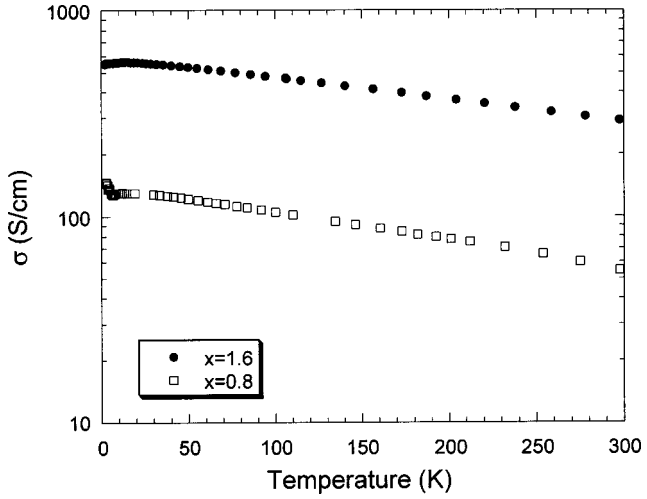

FIG. 7. Temperature dependence of the electrical conductivity of a $\sim 3 \times 3 \times 5$ mm^3 ingot sample of $K_2Bi_{8-x}Sb_xSe_{13}$ solid solutions for $x=0.8$ and 1.6.

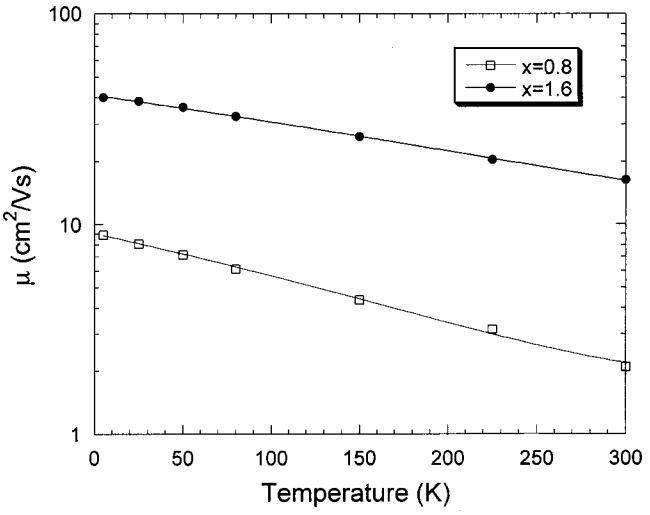

FIG. 9. Temperature dependence of mobility of the $K_2Bi_{8-x}Sb_xSe_{13}$ solid solutions for $x=0.8$ and 1.6.

excitation over the entire temperature range 4–300 K, Fig. 8.

The Hall mobility ($\mu_H = R_H \cdot \sigma$) at room temperature was greater for the $x=1.6$ sample ($\sim$16 cm^2/Vs) than for $x=0.8$ ($\sim$2 cm^2/Vs), Fig. 9. This explains the main difference in the electrical conductivity (factor >5) between the two members. As expected, for a degenerate semiconductor or a metal, the mobilities increase at lower temperature and this is responsible for the observed metallike temperature dependence of the electrical conductivity. Overall, the Hall mobilities are relatively low and indicate the existence of many defects and other scattering centers in these ingots. At this stage, it is unclear what the nature and extent of these defects are. Possible sources include the substitutional mass fluctuation disorder between K/Bi/Sb in the structure, atom vacancies, as well as positively charged potassium atoms (which exhibit static positional disorder).[11] The role of these scattering carriers needs to be understood. Also, macroscopic imperfections in the ingots such as grain boundaries and interneedle spaces (see Fig. 5) could influence dramatically the mobility and thus the electrical conductivity.[16]

Thermoelectric power measurements on $K_2Bi_{8-x}Sb_xSe_{13}$ solid solutions were also carried out along the needle direction for the members $x=0.8$ and $x=1.6$. The Seebeck coefficients are negative in value and become less negative as the temperature is decreased from room temperature down to 4 K, consistent with highly doped *n*-type semiconductors, see Fig. 10. The Seebeck coefficients at room temperature were -127 μV/K for $x=0.8$ and -100 μV/K for $x=1.6$.

F. Thermal conductivity

The mass fluctuation generated in the lattice of $K_2Bi_8Se_{13}$ by the mixed occupation of Sb and Bi atoms is expected to reduce the lattice thermal conductivity. The lattice thermal conductivity (κ_l) can be obtained by subtracting the electronic contribution (κ_e) from the total thermal conductivity.[17] The latter can be estimated by applying the

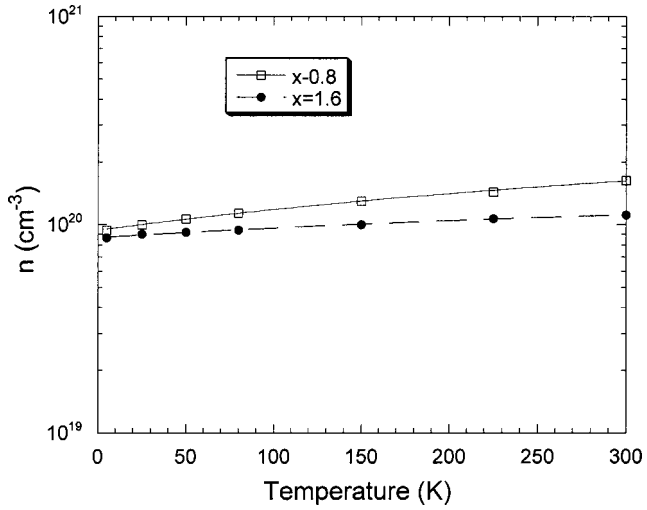

FIG. 8. Temperature dependence of carrier concentration of the $K_2Bi_{8-x}Sb_xSe_{13}$ solid solutions for $x=0.8$ and 1.6.

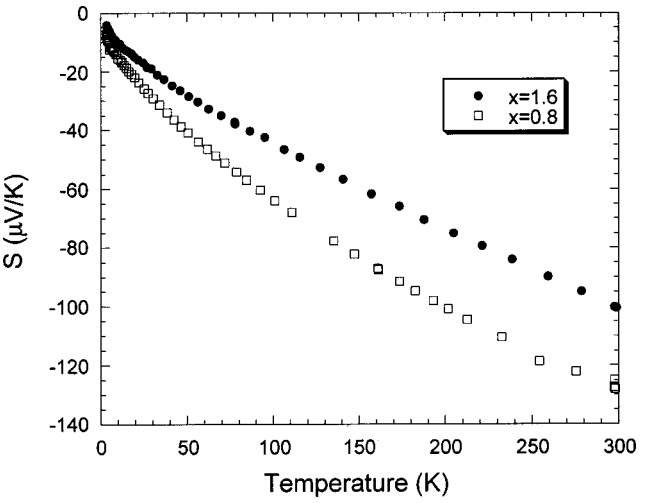

FIG. 10. Temperature dependence of Seebeck coefficient of a $\sim 3 \times 3 \times 5$ mm^3 ingot sample of $K_2Bi_{8-x}Sb_xSe_{13}$ solid solutions for $x=0.8$ and 1.6.

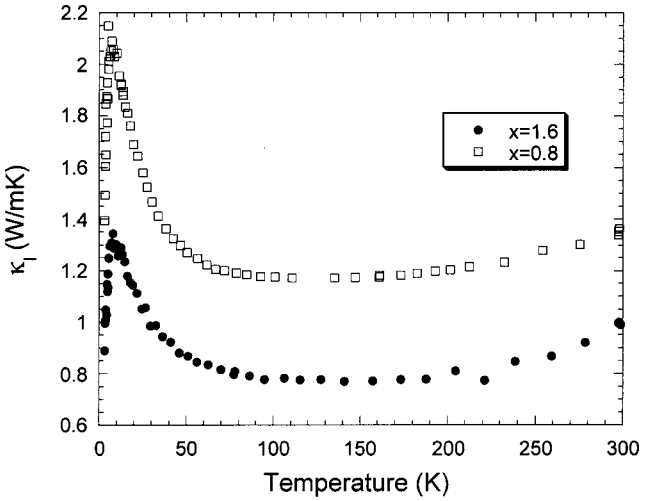

FIG. 11. Temperature dependence of lattice thermal conductivity of the $K_2Bi_{8-x}Sb_xSe_{13}$ solid solutions for $x=0.8$ and 1.6.

Wiedemann–Franz Law, $\kappa_e=\sigma\cdot L\cdot T$, where L is the Lorenz number taken[18] to be $\sim 2.44\times 10^{-8}$ V^2/K^2, σ is the electrical conductivity, and T is the temperature.

Lattice thermal conductivity of both members of solid solutions, see Fig. 11, exhibit a peak at ~7 K, which is caused by the competition between the phonon–boundary scattering and umklapp phonon–phonon interactions.[18] The peak is suppressed for $x=1.6$ due to the increased disorder in the heavy metal sites compared to $x=0.8$.

The measured thermal conductivity was 1.4 and 1.2 W/m K for $x=0.8$ and 1.6 at room temperature, respectively, and the lattice thermal conductivities (estimated after Wiedemann–Franz corrections) decrease from 1.36 W/m K for $x=0.8$ to 1.0 W/m K for $x=1.6$, Fig. 11. The lattice thermal conductivity is estimated to be as low as ~1.1 W/m K for $x=0.8$ and ~0.6 W/m K for $x=1.6$ after correction of the measured thermal conductivity for radiation losses based on $\sim T^3$ law.[19] These values are lower than Bi_2Te_3 that possesses lattice thermal conductivity below 1.5 W/m K and optimized $Bi_{2-x}Sb_xTe_3$ solid solutions possess values below 1 W/m K.[20]

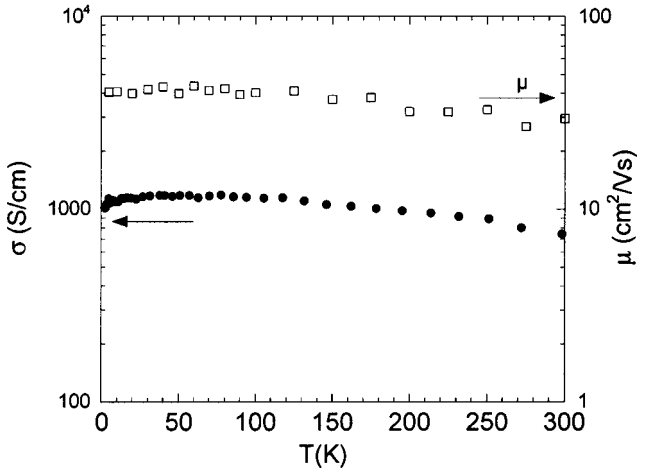

FIG. 12. Electrical conductivity and mobility of $\sim 3\times 3\times 5$ mm^3 ingot sample of $K_2Bi_{8-x}Sb_xSe_{13}$ ($x=1.6$) with 0.2% Se excess.

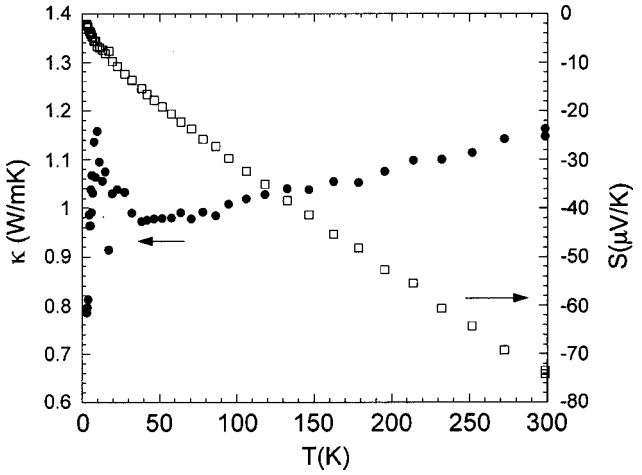

FIG. 13. Seebeck coefficient and thermal conductivity of $\sim 3\times 3\times 5$ mm^3 ingot sample of $K_2Bi_{8-x}Sb_xSe_{13}$ ($x=1.6$) with 0.2% Se excess.

G. Doping studies

The experimental data discussed herein on the selected members of the $K_2Bi_{8-x}Sb_xSe_{13}$ system indicate that these samples possess many defects that resulted in high carrier concentration and low mobility. We surmised that a possible source of these defects in the ingot could be the loss of some Se due to vaporization during sample preparation. This loss would create atom vacancies that could contribute two extra electrons to the conduction band as well as act as scattering centers. To explore this possibility, ingots doped with a compensating 0.2 wt % Se excess were prepared and studied. Additionally, in an attempt to increase the power factor, preliminary doping studies were carried out using dopants such as Pb and Sn in different concentrations on oriented ingots of $K_2Bi_{8-x}Sb_xSe_{13}$ ($x=1.6$). This member was selected because it possessed the lowest lattice thermal conductivity among the samples examined.

H. $K_2Bi_{8-x}Sb_xSe_{13}$ doped with excess of Se

An oriented ingot of $K_2Bi_{8-x}Sb_xSe_{13}$ ($x=1.6$) was prepared with 0.2 wt % excess Se added in the reaction mixture. The electrical conductivity measurements along the growth direction gave a significantly higher value of 746 S/cm at room temperature compared to 292 S/cm for the same member with no Se added, see Figs. 12 and 7. Hall effect measurements for samples with 0.2 wt % Se excess gave a carrier concentration of about 1.7×10^{20} cm^{-3} and an increased Hall mobility of ~30 cm^2/Vs. The weak temperature dependence of Hall mobility is shown in Fig. 12.

The Seebeck coefficient decreased with the addition of 0.2 wt % Se from ~−100 to ~−74 μV/K, Fig. 13, and this can be attributed to the increase in carrier concentration. Thermal conductivity along the needle direction of the sample ($x=1.6$) with Se excess was 1.16 W/m K at room

TABLE I. Electrical conductivity, Seebeck coefficient, power factor ($S^2\sigma$), thermal conductivity, and *ZT* at 300 K and extrapolated power factor and *ZT* at 500 K of doped $K_2Bi_{8-x}Sb_xSe_{13}$ ($x=1.6$).

Dopant (mol %)	σ (S/cm)	S (μV/K)	$S^2\sigma$ (μW/cm K^2)	κ (W/m K)	*ZT*	$S^2\sigma_{500\ K}$ (μW/cm K^2)	$ZT_{500\ K}$
···	292	−100	2.92	1.21	0.07	4.3	0.18
0.05 Pb	375	−78	2.28	0.84	0.08	3.1	0.19
0.10 Pb	188	−86	1.39	1.02	0.04	2.0	0.10
0.50 Pb	42	−82	0.28	1.02	0.01	0.4	0.02
1.00 Pb	78	−75	0.44	0.96	0.01	0.6	0.03
0.20 Sn	1096	−79	6.24	1.08	0.17	9.6	0.45
0.50 Sn	540	−87	4.09	1.32	0.09	4.0	0.15
1.00 Sn	638	−64	2.61	1.25	0.06	4.2	0.17

temperature (Fig. 13). The power factor increased by factor of ~1.4 and overall, the *ZT* of this sample increased by a factor of ~1.4.

A similar increase in *ZT* was observed in the $x=0.8$ member when excess Se was added. The electrical conductivity increased dramatically at room temperature rising from 55 S/cm in the original sample to 495 S/cm in the sample with 0.2 wt % Se excess added. Hall effect measurements show that the increasing electrical conductivity is dominated by the significant increase of mobility (~18 cm^2/V s, increasing by a factor of ~9) rather than the increase in carrier concentration (similar room temperature value of $\sim 1.7\times10^{20}$ cm^{-3}). Although the Seebeck coefficient decreased from −127 to −92 μV/K, the power factor increased significantly by a factor of ~5. The thermal conductivity of the sample with Se excess was ~1.3 W/m K at room temperature, relatively unchanged from the previous value. Overall, the *ZT* in this sample increased spectacularly by a factor of 5, mainly due to the significant increase in electrical conductivity and the absence of significant losses in Seebeck coefficient.

For both samples, the hypothesis of the high carrier concentration observed in the as-prepared samples does not seem to be valid. It would appear that Se doping plays a more complex role since it does not significantly affect the carrier concentration, yet, it results in a marked increase in Hall mobility (factor of ~2 for $x=1.6$ and ~9 for $x=0.8$). In any case, these results suggest that Se excess may be an important mechanism for defect elimination and therefore Se doping could be an interesting and effective way to control the properties in these materials.

I. Doped $K_2Bi_{8-x}Sb_xSe_{13}$ ($x=1.6$) with Pb and Sn

$K_2Bi_{8-x}Sb_xSe_{13}$ ($x=1.6$) was selected to examine how sensitively it responds to the addition of ''external'' impurities using dopants such as Sn and Pb. The doping concentrations used and results obtained are presented in Table I. The charge-transport properties of these doped materials were measured along the needle direction on grown ingots. For all doping concentrations employed, the Seebeck coefficient of the samples was lower than in the undoped versions of $K_2Bi_{8-x}Sb_xSe_{13}$ ($x=1.6$). This is consistent with the small increase in carrier concentration in the doped samples. Electrical conductivity values in the doped samples gave a minimum of 42 S/cm at room temperature using 0.5 mol % Pb as dopant, and a maximum of 1096 S/cm using 0.2 mol % Sn. We believe that the variation in the electrical conductivity of the doped samples vis-à-vis undoped is attributed not only to changes in carrier concentration but also changes in mobility. Interestingly, the thermal conductivity of all samples remained relatively unchanged, see Table I. A promising power factor of 6.24 μW/cm K^2 was obtained for the sample doped with 0.2 mol % Sn, which gives *ZT* of 0.17 at room temperature.

The trend of the power factor and *ZT* in all samples is to increase substantially at higher temperatures, mainly due to the continued increase of the Seebeck coefficient. Indeed, preliminary measurements[21] up to 700 K indicate that the Seebeck coefficient keeps increasing almost linearly without a slope change. This gives a strong reason to extrapolate the data at higher temperature and estimate the power factor and the *ZT*. This was performed based on a quadratic fitting of the resistivity and linear fitting of Seebeck coefficient. Table I includes the extrapolated values for all doped samples at 500 K. *ZT* as high as 0.45 is predicted for $K_2Bi_{8-x}Sb_xSe_{13}$ ($x=1.6$) with 0.2% Sn. These results suggest that we should consider these materials promising for high-temperature applications. However, measurements at higher temperatures (i.e., 300–700 K) need to be done.

J. Anisotropy of thermoelectric properties: Measurements perpendicular to the growth axis

Because the $K_2Bi_{8-x}Sb_xSe_{13}$ materials are highly anisotropic in structure and morphology, it is of interest to evaluate their transport properties in different growth directions. Therefore, we performed electrical conductivity, Seebeck coefficient, thermal conductivity, and Hall effect measurements on the member $x=1.6$ of $K_2Bi_{8-x}Sb_xSe_{13}$ parallel and perpendicular to the growth direction (i.e., crystallographic *b* axis).

Electrical conductivity measurements along both directions, as a function of temperature, showed spectacular anisotropy, see Fig. 14(a). The room-temperature value along the needle direction was ~292 S/cm, about five times larger than perpendicular to it at ~59 S/cm. Seebeck coefficients on the same sample parallel and perpendicular to the needle direction showed much less anisotropy with room-temperature values of −100 μV/K and −84 μV/K, respectively, see Fig. 14(b).

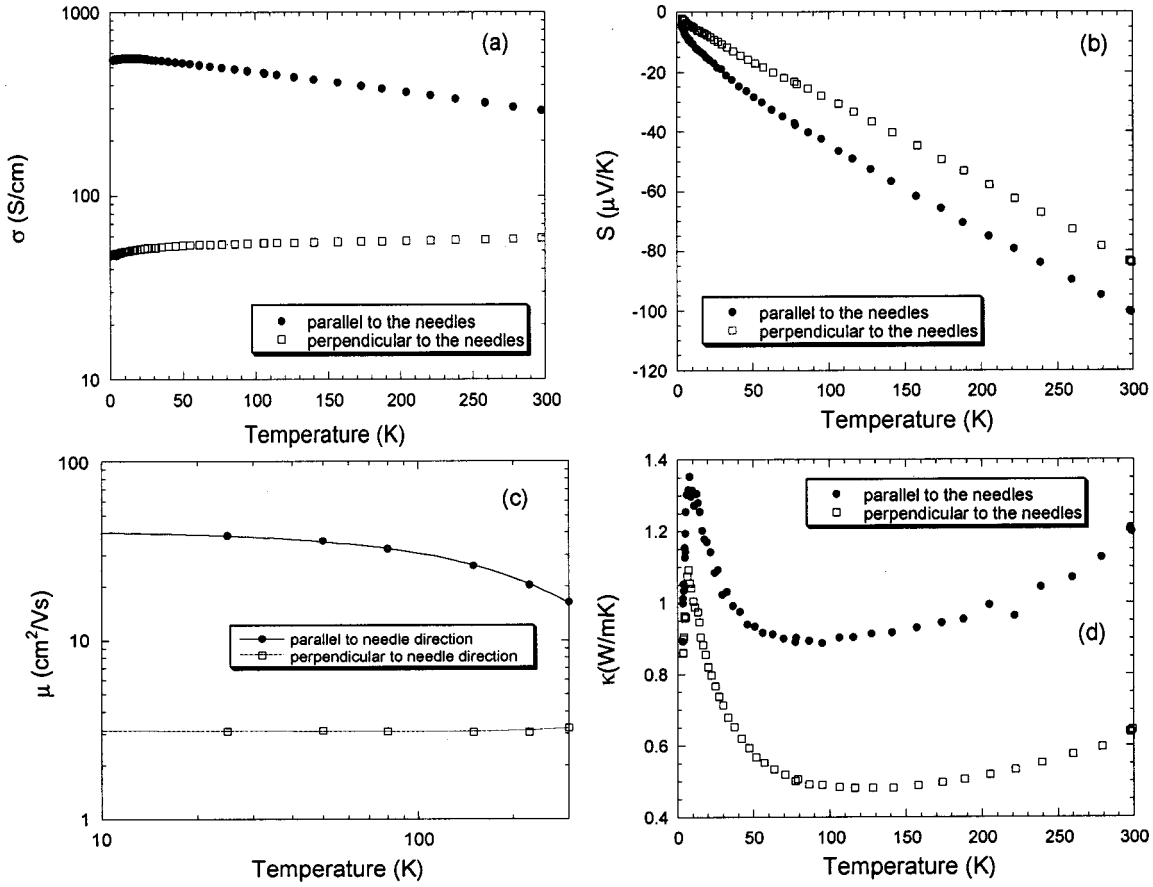

FIG. 14. (a) Electrical conductivity, (b) Seebeck coefficient, (c) Hall mobility, and (d) thermal conductivity of a $\sim 3\times 3\times 5\ \mathrm{mm}^3$ ingot sample of $K_2Bi_{8-x}Sb_xSe_{13}$ ($x=1.6$) parallel and normal to the needle direction with temperature.

The Hall mobilities parallel and perpendicular to the needle direction were $\sim 16\ \mathrm{cm}^2/\mathrm{V\,s}$ and $\sim 3\ \mathrm{cm}^2/\mathrm{V\,s}$, respectively, at room temperature, Fig. 14(c). Thus, the mobility drops significantly when current flows perpendicular to the needles. This could be due to heavier carrier effective masses[22] in this direction and boundary scattering, caused by the interneedle space and/or microcracks. The microcracks could be present because of easy cleavage along the needle direction. The strong anisotropy in mobility causes the significant anisotropy in the electrical conductivity in the two directions. The weak temperature dependence of the mobility and the different slopes in the two directions suggest an anisotropic mixed scattering mechanism that affects the conductivity, as well as the Seebeck coefficient. However, the anisotropy in the Seebeck coefficient is much less compared to that of the electrical conductivity.

For a single-band model, the electrical conductivity e.g., along the x is given by,[23]

$$\sigma_x=\frac{2ne^2}{3m_x}\cdot\frac{\int_0^\infty \frac{\partial f}{\partial \epsilon^*}(\epsilon^*)^{3/2}\tau_x(\epsilon^*)d\epsilon^*}{F_{1/2}(\eta)}, \tag{1}$$

while the Seebeck coefficient is given by

$$S_x=-\frac{k_B}{e}\left[\frac{\int_0^\infty \frac{\partial f}{\partial \epsilon^*}(\epsilon^*)^{5/2}\tau_x(\epsilon^*)d\epsilon^*}{\int_0^\infty \frac{\partial f}{\partial \epsilon^*}(\epsilon^*)^{3/2}\tau_x(\epsilon^*)d\epsilon^*}-\eta\right], \tag{2}$$

where k_B is the Boltzman constant, m^* is the effective mass, ϵ^* is the reduced energy (ϵ/k_BT), $\tau(\epsilon^*)$ is the relaxation time, f is the distribution function, η is the reduced Fermi energy (ϵ_F/k_BT), and $F_{1/2}(\eta)$ is the Fermi integral

$$F_{1/2}(\eta)=\int_0^\infty \frac{x^{1/2}dx}{1+\exp(x-\eta)}. \tag{3}$$

From Eqs. (1)–(3), it is clear that for conduction along the x direction in an anisotropic material, the electrical conductivity depends strongly on the effective mass ($\sim 1/m_x$) and the relaxation time along x. In contrast, the Seebeck coefficient is not directly affected by the effective mass. Although it depends on the relaxation time, according to Eq. (2) the dependence involves the ratio of $\tau(\epsilon^*)$ containing integrals; thus, the influence of relaxation time is severely damped. This argument is consistent with the observed experimental data here, where the electrical conductivity ratio along ($\sigma_\parallel$) and perpendicular ($\sigma_\perp$) to the needle direction is ~ 5 while the same ratio of Seebeck coefficient is only ~ 1.1.

A substantial anisotropy was also observed in the thermal transport properties of this sample (i.e., $x=1.6$) The thermal conductivity perpendicular to the needle axis is only about half that in the parallel direction. Thus, the room-temperature value in the perpendicular direction is extremely low at 0.64 W/m K, Fig. 14(d).

Thermal conductivity anisotropy is caused by the contribution of two terms, the electronic and lattice. The electronic contribution is given by the Wiedemann–Franz law ($\kappa_{el}=\sigma\cdot L\cdot T$) and is affected by the electrical conductivity and the Lorenz factor anisotropy. The Lorenz factor along x direction is given[23] by:

$$L_x=\frac{k_B^2}{e^2}\frac{\int_0^\infty \frac{\partial f}{\partial \epsilon^*}(\epsilon^*)^{3/2}\tau_x(\epsilon^*)d\epsilon^*\cdot\int_0^\infty \frac{\partial f}{\partial \epsilon^*}(\epsilon^*)^{7/2}\tau_x(\epsilon^*)d\epsilon^*-\left[\int_0^\infty \frac{\partial f}{\partial \epsilon^*}(\epsilon^*)^{5/2}\tau_x(\epsilon^*)d\epsilon^*\cdot\right]^2}{\left[\int_0^\infty \frac{\partial f}{\partial \epsilon^*}(\epsilon^*)^{3/2}\tau_x(\epsilon^*)d\epsilon^*\right]^2}, \tag{4}$$

and since again the dependence involves the ratio of integrals, the influence of the relaxation time is weak. The simplest approach for the lattice contribution in the thermal conductivity, according to Debye, is given[23] by:

$$\kappa_l=\tfrac{1}{3}C\cdot v\cdot \ell, \tag{5}$$

where C is the specific heat per unit volume, v is the average phonon velocity, and ℓ is the average mean free path of a phonon both of which depend of crystallographic direction.

When heat propagates parallel to the needle axis of $K_2Bi_{8-x}Sb_xSe_{13}$, it flows through the relatively regular Bi_2Te_3-type and NaCl-type rods (Fig. 4), which present an extended but regular medium made of Bi—Se bonds. Along the needle axis, the lattice constant b is only ~4.2 Å which favors a relatively long mean-free phonon path. In contrast, when heat propagates in the perpendicular direction, which is the direction of a large lattice constant ($a\sim 17$ Å, $c\sim 18$ Å), the acoustic phonons strongly scatter from the K^+ ions and the high coordinated sites $K(1)$ and $M(8)$ that serve as barriers and interrupt the Bi/Sb/Se framework. This considerably shortens the mean-free path and severely suppresses the thermal conductivity. Because the very low thermal conductivity perpendicular to the needles is offset by the even lower electrical conductivity, the direction of maximum ZT is still that of the needle axis.

IV. CONCLUSIONS

At small x values (i.e., $x<2$) the energy gap of the $K_2Bi_{8-x}Sb_xSe_{13}$ solid solutions showed an anomalously minimum value that is related to the preference of Sb to substitute specific K-containing sites in the structure. It is believed that this site preference also influences the thermoelectric properties of these materials. No eutectic compositions were observed. The lattice thermal conductivity decreases due to the mass fluctuation caused by the Sb incorporation in the lattice. Doping experiments using various dopants showed that it is possible to further improve the power factor in these materials. Furthermore, extrapolation of power factor and ZT suggested that they are more suitable for high-temperature applications. Detailed measurements at this temperature range are planned. Measurements in directions parallel and perpendicular to the growth axis showed a strong anisotropy in the charge-transport properties and thermal conductivity. Future studies in these needlelike materials should be done along the needle direction as suggested by the significantly higher overall thermoelectric performance. The well-oriented polycrystalline samples of the $K_2Bi_{8-x}Sb_xSe_{13}$ solid solutions showed promising thermoelectric properties. Crystal growth needs to be improved further in order to enhance needle width and reduce interneedle grain boundaries, which should lead to even higher mobilities and enhanced power factors.

ACKNOWLEDGMENTS

The authors thank Professor S. D. Mahanti (Michigan State University) and Professor E. Hatzikraniotis (Aristotle University of Thessaloniki, Greece) for fruitful discussions. Financial support from the Office of Naval Research (Contract No. N00014-01-1-0728) and DARPA (M.G.K. and C.U.) is gratefully acknowledged. The work made use of the SEM facilities of the Center for Electron Optics at Michigan State University.

[1] $Z\cdot T=(S^2\sigma/\kappa)\cdot T$, where σ is the electrical conductivity, S is the Seebeck coefficient, κ is the thermal conductivity, and T is the temperature.
[2] N. F. Mott and H. Jones, *The Theory of the Properties of Metals and Alloys* (Dover, New York).
[3] G. A. Slack, in *CRC Handbook of Thermoelectrics*, edited by D. Rowe (CRC Press, Boca Raton, FL, 1995), pp. 407–440; G. A. Slack, in *Solid State Physics*, edited by H. Ehrenreich, F. Seitz, and D. Turnbull, (Academic, New York, 1997), Vol. 34, p. 1.
[4] M. G. Kanatzidis, Semicond. Semimetals **69**, 51 (2000); D.-Y. Chung, L. Iordanidis, K.-S. Choi, and M. G. Kanatzidis, Bull. Korean Chem. Soc. **19**, 1283 (1998).
[5] A. Mrotzek, D.-Y. Chung, N. Ghelani, T. Hogan, and M. G. Kanatzidis, Chem.-Eur. J. **7**, 1915 (2001); K.-S. Choi, D.-Y. Chung, A. Mrotzek, P. Brazis, C. Kannewurf, C. Uher, W. Chen, T. Hogan, and M. G. Kanatzidis, Chem. Mater. **13**, 756 (2001); A. Mrotzek, D.-Y. Chung, T. Hogan, and M. G. Kanatzidis, J. Mater. Chem. **10**, 1667 (2000).
[6] D.-Y. Chung, K.-S. Choi, L. Iordanidis, J. L. Schindler, P. M. Brazis, C. R. Kannewurf, B. Chen, S. Hu, C. Uher, and M. G. Kanatzidis, Chem. Mater. **9**, 3060 (1997).
[7] P. W. Brazis, M. Rocci-Lane, J. R. Ireland, D.-Y. Chung, M. G. Kanatzidis, and C. R. Kannewurf, *Proceedings of the 18th International Conference on Thermoelectrics* (IEEE, Baltimore, MD, 1999), p. 619.
[8] T. Kyratsi, D.-Y. Chung, K.-S. Choi, J. S. Dyck, W. Chen, C. Uher, and M. G. Kanatzidis, Mater. Res. Soc. Symp. Proc. **626**, Z8.8.1 (2000).
[9] W. W. Wendlandt and H. G. Hecht, *Reflectance Spectroscopy* (Interscience Publishers, New York, 1966); G. Kotum, *Reflectance and Spectroscopy*

(Springer, New York, 1969); S. P. Tandon and J. P. Gupta, Phys. Status Solidi **38**, 363 (1970).
[10] CERIUS^2, Version 2.35; Molecular Simulations Inc, Cambridge, UK, 1995.
[11] T. Kyratsi, D.-Y. Chung, and M. G. Kanatzidis, *J. Alloys Compds* (unpublished).
[12] J. Black, E. M. Conwell, L. Seigle, and C. W. Spencer, J. Phys. Chem. Solids **2**, 240 (1957).
[13] Landolt–Borstein, *Numerical Data and Functional Relationships in Science and Technology*, edited by O. Madelung (Springer, Berlin, 1983), Vol. 17f, Sb_2Se_3 p. 256, Bi_2Te_3 p. 272, $Bi_{2-x}Sb_xTe_3$ p. 279, and references therein.
[14] M. Evain, U-FIT: *A cell parameter refinement program*, Institut des Materiaux de Nantes, Nantes, France (1992).
[15] P. Brazis, J. Ireland, M. Lane, T. Kyratsi, D.-Y. Chung, M. G. Kanatzidis, and C. R. Kannewurf, Mater. Res. Soc. Symp. Proc. **626**, Z.8.11.1 (2000).
[16] In Ref. 6, β-$K_2Bi_8Se_{13}$ electrical conductivity measured on ingot is ~30 S/cm, while the electrical conductivity measured on single crystal is ~250 S/cm. This significant difference is attributed to macroscopic imperfections of the ingot.
[17] The thermal conductivity has two contributions, one from carrier (κ_{el}), which is directly proportional to the electrical conductivity by Wiedeman–Franz law, and the other from the lattice (κ_{lat}), which is related to lattice structure. This assumes that the data do not include radiative loss effects. In this case, a correction for radiative losses has to be made.
[18] C. Kittel, *Introduction to Solid State Physics*, 6th Ed. (J. Wiley, New York, 1986), p. 150.
[19] L. Genzel, Z. Phys. **135**, 177 (1953).
[20] H. J. Goldsmid, in *Materials Used in Semiconducting Devices*, edited by C. A. Hogarth (J. Wiley, London, 1965), p. 165.
[21] Seebeck measurements of ingots of $K_2Bi_8Se_{13}$-based materials up to 700 K show a straight linear propagation of the thermopower without signs of saturation and reversal; T. Kyratsi and M. G. Kanatzidis (unpublished).
[22] Band structure calculations suggest that effective mass in the direction perpendicular to the needles is heavier than that along the needle direction; P. Larson, Ph.D dissertation, Michigan State University, 2001.
[23] V. I. Fistul, *Heavily Doped Semiconductors* (Plenum, New York, 1969).